IAEA nuclear fusion

Anomalous transport of light and heavy impurities in Tore Supra ohmic, weakly sawtoothing plasmas

To cite this article: R. Guirlet *et al* 2009 *Nucl. Fusion* **49** 055007

Nucl. Fusion 49 (2009) 055007 (9pp) doi:10.1088/0029-5515/49/5/055007

Anomalous transport of light and heavy impurities in Tore Supra ohmic, weakly sawtoothing plasmas

R. Guirlet, D. Villegas, T. Parisot[a], C. Bourdelle, X. Garbet, F. Imbeaux, D. Mazon, D. Pacella[b]

CEA, IRFM, F-13108 Saint-Paul-Lez-Durance, France

Received 17 November 2008, accepted for publication 18 March 2009
Published 9 April 2009
Online at stacks.iop.org/NF/49/055007

Abstract
Experimental results on impurity transport in tokamaks are based on various techniques. We study here how the choice of the injection technique and of the analysis method influences the results. We have used three different injection techniques available in Tore Supra: laser blow-off, gas puff and supersonic molecular beam injection. We show that the long time duration of the gas puff injection compared with particle confinement time provides very limited information. The laser blow-off technique and supersonic pulsed injections give satisfactory results for diffusion but low quality convection estimates, presumably because the fast source term quenches the role of convection in the continuity equation. The best method is shown to be the combined analysis of supersonic pulsed injections and continuous puffing of a gaseous species. We obtain convection velocity profiles to an uncertainty of about $0.5\,\mathrm{m\,s^{-1}}$. This method is applied to ohmic, weakly sawtoothing plasmas. The diffusion coefficient is independent of the impurity charge and the convection velocity is inward. Neoclassical calculations show that these plasmas are dominated by anomalous transport. Quasilinear gyrokinetic simulations are in qualitative agreement with the above experimental results. We deduce from the simulations that convection is dominated by the curvature term, which means that no charge dependence should be expected in this situation.

PACS numbers: 52.55.Fa, 52.25.Vy, 52.25.Fi, 52.35.Ra

(Some figures in this article are in colour only in the electronic version)

1. Introduction

Impurity transport in fusion devices plays a crucial role in the core performances of the plasma. In most experimental situations, it is reported that collisional (also called *neoclassical*) transport is not sufficient to interpret the observed impurity transport. However, as noticed in [1], the contribution of the so-called *anomalous* transport varies from one experiment to another. For example the centre of an L-mode plasma is found to be neoclassical (e.g. in TCV [2]) in some cases and anomalous (e.g. in JET [3]) in others. This anomalous transport has been attributed to turbulence. Recent publications have been dedicated to quantitative comparisons of models of turbulent transport [4–7] with experiments, with emphasis on the convection direction [8, 9] and the impurity charge dependence [10]. The reported results exhibit large differences between one another, which raises the question about the role of the wide variety of impurity injection techniques and analysis methods. There is thus no definite answer as to the ability of the models to reproduce the experimental results. This paper aims at providing material in the global process of critical assessment of modelling and experimental methods for impurity transport.

In this paper, the quality of the impurity transport determination is assessed for three different impurity injection techniques available in Tore Supra: laser blow-off, gas puffing and supersonic molecular beam pulsed injection (SMBI), evidencing the need for a fast technique when the convection velocity is to be determined accurately. In section 2 we describe the experimental scenario and the corresponding observations. In section 3 we describe the optimization of the experimental results using the available injection techniques and proposing various analysis methods. In section 4 the best method is applied to a comparison of experimental results with neoclassical and turbulent transport predictions in ohmic, weakly sawtoothing plasmas.

[a] Present address: Laboratoire Arc Electrique et Plasmas Thermiques, Universit Blaise Pascal, Clermont-Ferrand, France.
[b] Permanent address: Associazione Euratom-ENEA, Frascati, Italy.

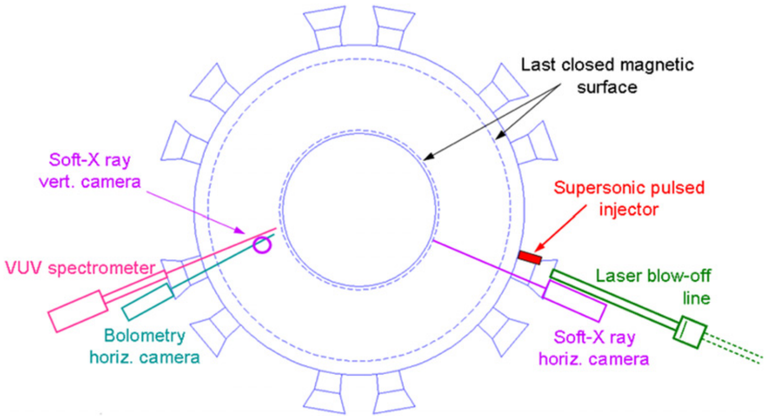

Figure 1. Schematic top view of the tokamak showing the trace impurity injectors and the diagnostics used for impurity measurements.

2. Experimental scenario and impurity injection techniques

We have performed a series of ohmic plasmas the main parameters of which are the following: major radius $R_0 = 2.38$ m, minor radius $a = 0.72$ m, plasma current $I_p = 0.5$ MA, safety factor at the last closed flux surface $q_\psi = 9.75$ and toroidal field $B_T = 3.87$ T. The central electron density is $n_e(0) = 2.6 \times 10^{19}$ m^{-3} and the central electron temperature is $T_e(0) = 1.9$ keV. The sawteeth, although not strictly absent from the plasmas, have a very small amplitude (the average temperature variation at a crash is 40 eV at the plasma centre) and exhibit a very central inversion radius $r/a = 0.1$. As our transport analysis is not sensitive to such small temperature differences we have retained this scenario which allows us to obtain good quality measurements. Nevertheless we keep in mind that the results concerning the central part of the plasma ($r/a \lesssim 0.12$) will be time averaged over several sawtooth periods. Total suppression of the sawteeth might have been achieved only by lowering even more the plasma current (and thus the electron density) at the expense of the measurement quality.

The main background plasma parameters for this study are the electron density and temperature. The electron density measurements used for impurity transport studies are performed by two reflectometers with a 1 cm spatial resolution and a 10-chord interferometer. The electron temperature measurements are performed by an ECE radiometer with 32 channels (2.5 cm spatial resolution). The reflectometers and the ECE radiometer cover the entire low field side of the plasma and a part of its high field side. All these diagnostics have a time resolution between 1 and 4 ms.

The impurity emission measurements (see figure 1) used to determine the transport coefficients are mainly those of a VUV spectrometer and a set of soft-x-ray cameras whose time resolution was set to 2 ms for the experiments described here. The soft-x-ray cameras are equipped with 50 μm thick Be filters corresponding to a cut-off energy of about 2 keV. They are located in a midplane port (45 chords) and a top port (37 chords) of the vessel. The VUV spectrometer has a fixed line of sight along a horizontal diameter of the plasma. It is sensitive in the wavelength range 10–100 nm. Since it is not absolutely calibrated in brightness, it was used only to monitor the time evolution of spectral lines emitted by each of the injected impurities:

- Nitrogen: N IV 76.5 nm, N V 24.7 nm
- Aluminium: Al IX 28.4 nm
- Chromium: Cr XI 23.5 nm, Cr XXI 15.0 nm
- Nickel: Ni XVII 24.9 nm, Ni XXV 11.8 nm
- Germanium: Ge XVI 12.2 nm, Ge XXII 22.6 nm

In addition, a set of horizontal bolometric lines of sight provides information on the injected impurity emission in the outer part of the plasma ($r/a \gtrsim 0.6$), where the soft-x-ray emission becomes negligible in these plasmas.

The laser blow-off injection system used in the present experiments (shown in figure 1) is described in detail in [12]. Four metallic impurities have been injected with this system: aluminium ($Z = 13$, discharge ♯38964), chromium ($Z = 24$, discharge ♯38966), nickel ($Z = 28$, discharge ♯38963) and germanium ($Z = 32$, discharge ♯38967). Differently from the situation of sawtooth-free, lower-hybrid wave heated plasmas previously analysed [12], the confinement time of these species (estimated from the decay time of the central soft-x-ray chord signal) is independent of the atomic number. Whether the previous result was due to a physics effect or to an analysis bias is not clear.

In order to extend the impurity charge range explored, we have performed supersonic pulsed injections of nitrogen ($Z = 7$) in an identical discharge (♯40783). As can be seen in figure 2, the common gas puff technique used in most previous studies of light species produces a source term longer than the particle confinement time (about 100 ms in Tore Supra), even when the valve opening duration is not longer than 20 ms. This is due to the conductance of the 1.5 m long pipe between the injection valve and the tokamak vessel. In order to obtain a short source term we have adapted the parameters of the SMBI (supersonic molecular beam injection) system located inside the vessel [11], initially designed for deuterium fuelling of the plasma, to trace impurity injections. The resulting source term, as illustrated in figure 2, is of a duration much shorter than a gas puff source term and similar to that due to a laser blow-off injection. It is interesting to note that this feature of the SMBI technique seems to persist for (at least) partially recycling species as we have found with argon ($Z = 18$) injections although with a long, weak tail of the source term

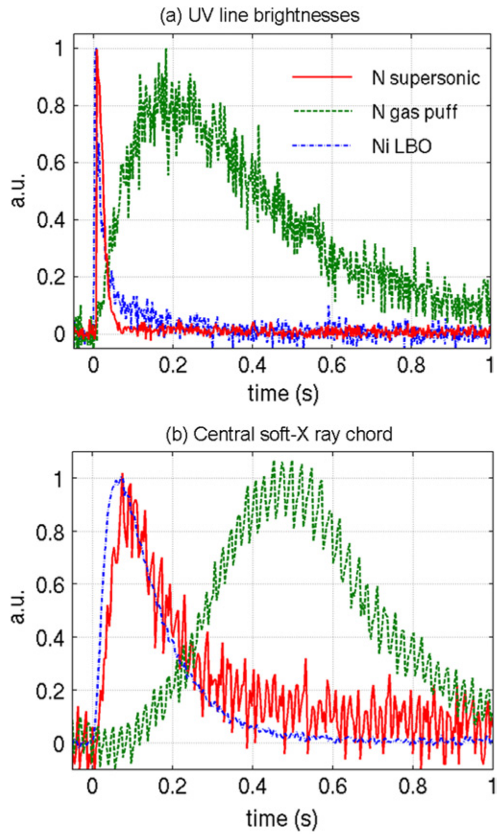

Figure 2. (*a*) Time evolution of peripheral line brightnesses (normalized to maximum) following impurity injections: N IV 24.92 nm following a *N* supersonic pulsed injection (solid red, pulse ♯40783), N IV 24.92 nm following a *N* gas puff (dashed green, ♯41028), Ni V following a Ni laser blow-off injection (dashed–dotted blue, ♯38963). (*b*) Injected impurity contribution to the central soft-x-ray brightness. Residual sawteeth are not taken into account in the analysis.

(estimated from the Ar VIII resonance line brightness) which we attribute to the argon recycling.

The supersonic pulsed injections can be set so that the background plasma is only weakly perturbed (the injector parameters are set so that n_e and T_e are not perturbed by more than 5% in the confined plasma) for a very short duration (a few milliseconds) before coming back to its initial state, while the impurity confinement time is of order 100 ms (in this regard, it makes the supersonic pulsed injections very similar to the laser blow-off injections). This allows us to assume that transport remains constant during almost the entire time interval of interest, while this assumption may not be valid for conventional gas puffs which perturb substantially the background plasma for several confinement times.

In addition to providing source terms much shorter than the characteristic transport time, this new technique allows repeated injections in the same pulse (in principle the number of injections is limited only by the plasma duration). This is an essential advantage to reduce the statistical uncertainties of the results without increasing the injected number of atoms above the trace level. The nitrogen results described in the following were obtained by averaging all measurements over four successive injections performed in the same plasma.

3. Experimental results

3.1. Radial transport analysis of laser blow-off injected species

The local transport analysis has been performed using the impurity radial transport code ITC [12] which solves the system of continuity equations for all the ionization stages of the injected element over the time interval when the injected impurity is present in the plasma core:

$$\frac{\partial n_Z}{\partial t} + \vec{\nabla}.\vec{\Gamma}_Z = S_{Z-1} + R_{Z+1} - (S_Z + R_Z) + \Sigma_Z,$$

where the subscript Z denotes the charge of the ionization stage, n_Z being its density, Γ_Z its flux, S_Z and R_Z its ionization and recombination rates respectively and Σ_Z the external source. The latter comprises the gas injection for the neutral state and losses in the scrape-off layer for all states. As usual in this kind of study, the impurity radial flux is supposed to be the sum of a diffusive term and a convective term:

$$\Gamma_Z(r) = -D(r)\nabla n_Z(r) + V(r)n_Z(r),$$

where $D(r)$ is the diffusion coefficient and $V(r)$ the convection velocity. We use the standard convention for V, i.e. V is positive when the convective flux is outward. The $D(r)$ and $V(r)$ coefficients are assumed not to depend on time since the background plasma is almost constant and the injected impurity is a trace. The one-dimensional nature of the ITC code imposes the hypothesis of toroidal and poloidal symmetries. These are probably verified for most ionization stages except the neutral and the first ionization stages. This is why we do not discuss the transport coefficients in the outer part of the plasma ($r/a > 0.8$).

The basic procedure has been described in [12]: the main input data to the code are the external source term, of which the time evolution is taken from a peripheral UV line brightness, and the electron density and temperature profiles over the time interval of interest, which are built from the interferometry and reflectometry measurements and from the ECE radiometer measurements, respectively. The ITC code starts from an initial guess of the transport coefficients radial profiles. After resolution of the coupled continuity equations ITC reconstructs the UV line, bolometric and soft-x-ray brightnesses according to measurements listed in the previous paragraph. This step is illustrated in figure 3 with a representative set of data corresponding to the Ni injection case. At the time of this analysis the brightness calibration of the soft-x-ray diagnostic was only relative (i.e. the radial shape of the profile was determined but not the absolute emission values). The bolometric signals were thus used in order to determine the absolute impurity densities. All the reconstructed soft-x-ray signals were multiplied by a single arbitrary factor chosen so that the simulated and measured maxima of the central chord match each other. As the UV spectrometer is not calibrated, the reconstructed line brightnesses are normalized to the measured maximum of each line of interest. ITC modifies iteratively the transport coefficients until the difference between the reconstructed signals and the measured ones is minimized in a χ^2 sense.

This procedure has been used for the analysis of the laser blow-off injected species. The resulting D and V profiles

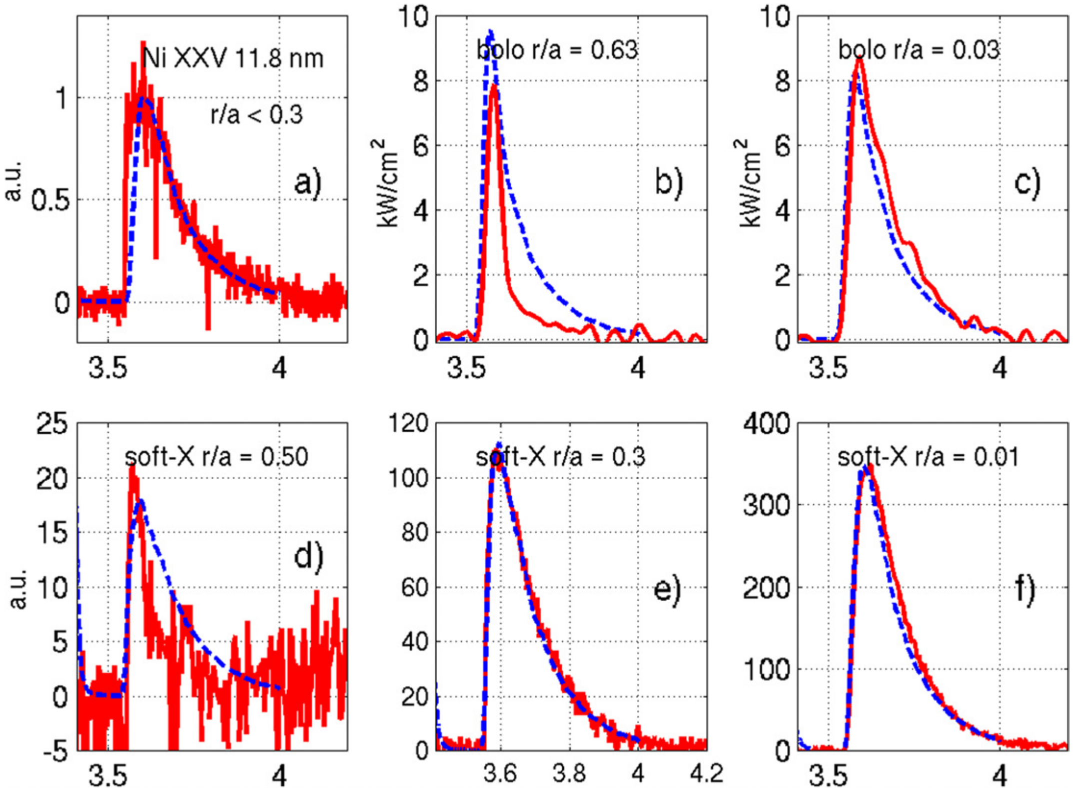

Figure 3. Measurements and simulations for a Ni injection (pulse ♯38963). (*a*) Ni xxv 11.8 nm, (*b*) and (*c*) bolometric chords at $r/a = 0.63$ and 0.03, respectively, (*d*), (*e*) and (*f*) soft-x-ray chords at $r/a = 0.50$, 0.30 and 0.01, respectively.

are shown in figure 4. The uncertainties indicated by the coloured bands have been obtained by varying the initial guess of the transport coefficient profiles and retaining all solutions corresponding to the minimal χ^2 within a 25% tolerance. This method of uncertainty determination aims at accounting for local minima.

It can be seen that the D profiles are affected by reasonable error bars (in the sense that the relative error is uniform along the minor radius and no sign change of the derivative is found within $r/a \leqslant 0.7$). On the contrary, the various species exhibit very different V profiles: sign variations along the radius can be seen (in particular for the V profile of Al), large uncertainties for certain points (Cr profile), but no trend in Z can be deduced from these differences. The convection velocity thus seems to suffer from a poorer determination than the diffusion coefficient, as already noticed in [12] in the case of a lower-hybrid heated plasma.

The weaker dependence of the impurity time evolution on convection has been explained in [13] by the $1/\sqrt{\omega}$ dependence of the convective term in the dimensionless continuity equation in the case of a periodic perturbation of frequency ω. In other words, the higher the frequency (or equivalently the faster the transient since any transient can be decomposed over a basis of periodical (sinusoidal) functions), the more difficult it is to determine V. The lesser role played by convection in rapidly evolving situations can be checked *a posteriori* in the present case by comparing the time evolution of the total injected impurity flux with the ones of the diffusive and convective fluxes. An example of these fluxes as modelled by the ITC code is shown in figure 5. It can be seen that in the fast initial phase of

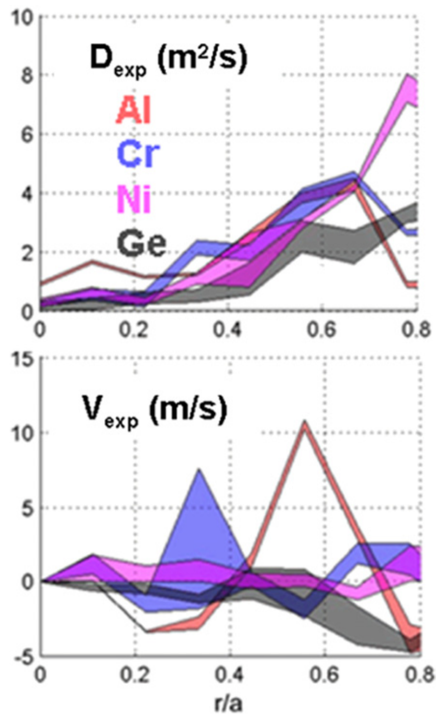

Figure 4. Radial profiles of (top) diffusion coefficient and (bottom) convection velocity for all laser blow-off injected species.

impurity penetration (for about 20–30 ms), the convective flux contributes very little to the total impurity flux compared with the slower decaying phase. This result holds at all positions in the plasma.

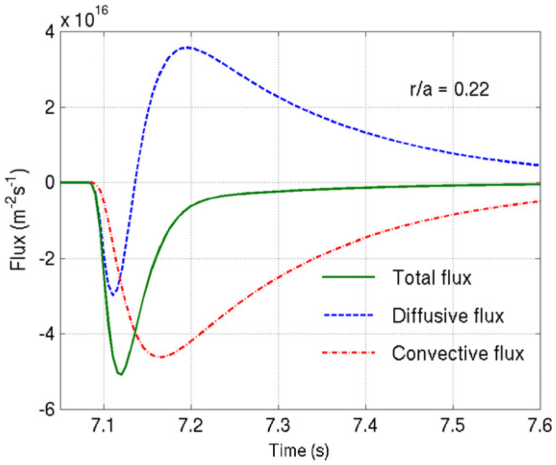

Figure 5. Total (green solid curve), diffusive (blue dashed curve) and convective (red dashed–dotted curve) N^{7+} fluxes at $r/a = 0.22$ as modelled by the ITC code in the nitrogen supersonic pulsed injection case (pulse ♯40783).

3.2. Assessment of the supersonic pulsed injection technique

As already said in section 2, the source duration corresponding to a supersonic pulsed injection is much shorter than the impurity confinement time. In order to assess the improvement in the transport coefficient determination using this technique with respect to the usual gas puff technique, the transport coefficients have been determined by means of the ITC code in both cases.

In order to make the comparison as clear as possible we have used the code in a different way. A family of D, V profiles was generated *a priori* within a domain (shown in figure 6) chosen from our experience in several different experimental scenarios. A compromise between computation time and radial resolution in D and V was made so that results such as those shown on the figure can be obtained in a few hours without optimizing the computation techniques. To save even more time we have constrained the D profiles to be monotonically increasing from the plasma centre to the edge, a hypothesis in agreement with most observations in ohmic and L-mode plasmas [12, 14]. We have also constrained the convection velocity to be inward (negative) and convexe, for the same reasons and for theoretical reasons discussed in section 4. The code has been run for all pairs of D and V profiles. All those pairs giving a χ^2 less than $1.33 \times \chi^2_{\rm min}$ are retained, the other ones being rejected.

The resulting D and V are shown in figure 6 in the form of coloured areas encompassing all retained profiles. The D band is strikingly narrower in the SMBI case, which confirms the advantage of this technique over the gas puff technique. It is to be noticed that this narrow band is not completely included in the broad band of the gas puff case. It is difficult to determine the exact reason for this inconsistency, but it has to be said that, besides the fact that the error bars defined in the way described above depend on the choice of the χ^2 criterion, the role of measurement uncertainties in the data has not been investigated.

As far as V is concerned, the improvement of the SMBI technique over the gas puff technique is moderate. As for the laser blow-off injections (see section 3.1), this is attributed to the weak sensitivity of a fast transient time evolution to the convective term, as discussed in section 3.1.

3.3. Method optimization for transport coefficient determination

In order to improve the V determination, we have performed a combined analysis of a nitrogen transient case (supersonic pulsed injection of N_2, ♯40783) and of a nitrogen stationary case (continuous N_2 puffing, ♯40866). The former case provides the diffusion coefficient profile with a satisfying uncertainty, as shown in the previous paragraph, while we deduce from the latter case the radial profile of the transport coefficient ratio V/D (D and V cannot be determined separately in this case since the continuity equation takes the form $\nabla n/n = V/D$).

For this purpose we have used the ITC code for the transient case as explained in section 3.1, which means in particular that no constraints were imposed on either D or V. The best D profile is then used as a constraint when ITC is used on the stationary case, while the V profile is adjusted until the χ^2 reaches a minimum. A couple of iterations between the two cases ensure that a solution suitable for both is found.

The results are shown in figure 7 as darker bands, while the results of the analysis of the transient case alone are shown for comparison in lighter colours. In both cases the error bands are obtained by varying the profiles around the solution and retaining those with a satisfactory χ^2. The error bar drops from 1 to 1.5 m s^{-1} in the case of the transient alone down to 0.5 m s^{-1} with the combined analysis. Note that with the latter method the final V does not change sign along the minor radius, in contrast to the transient case alone (and to the laser blow-off injected species discussed in section 3.1). For this reason, and for the methodological reasons explained above, we consider the combined analysis as giving more credible results than that of a transient alone.

3.4. Results on transport coefficients

As can be seen in figures 4 and 6, the diffusion coefficient values are similar to the case of sawtooth-free plasmas obtained by lower-hybrid current drive (LHCD) [12], but here D increases smoothly and monotonously from the centre to the plasma periphery (in the LHCD case, there is a sharp transition around $r/a = 0.3$). The error bars do not allow us to evidence a D dependence on the impurity charge, although it has to be noticed that the nitrogen (the lightest species in this study) diffusion coefficient lies at the lower limit of the uncertainties over the central plasma region. As far as convection is concerned, the only profile we consider reliable enough is that of nitrogen, for the reasons explained above. It is entirely negative (i.e. convection is inward everywhere) and in the range of a few meters per second with an error bar of about 0.5 m s^{-1}. These results will now be compared with simulations of neoclassical and turbulent impurity transport.

4. Theoretical transport modelling

4.1. Neoclassical transport

The neoclassical diffusion coefficient and convection velocity have been calculated using the NCLASS code [15].

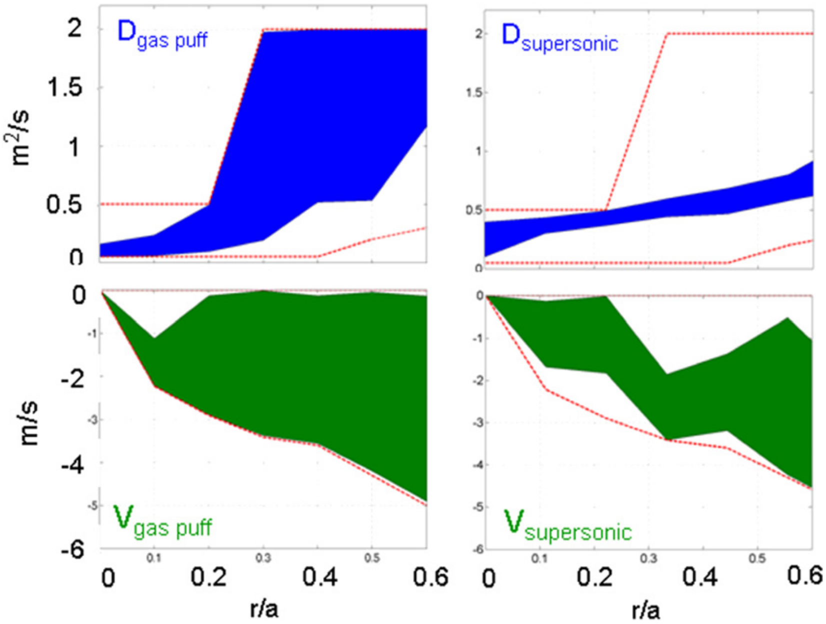

Figure 6. Radial profiles of (top) diffusion coefficient and (bottom) convection velocity for nitrogen (left) gas puff injection and (right) supersonic pulsed injection. Dotted red line: limits of allowed domains of variation. Detailed explanations in the text.

The NCLASS simulations use input profiles resulting from current diffusion simulations by the CRONOS code [17]. CRONOS uses T_e profiles fitted from the ECE and Thomson scattering measurements and n_e profiles fitted from the reflectometry and interferometry measurements. The T_i profile is evaluated by CRONOS with the constraint to match the carbon temperature measured by six lines of sight of charge exchange recombination spectroscopy, the total plasma energy and the measured neutron rate from the D-D reactions. In the NCLASS calculations the typical intrinsic impurity content is assumed, namely 5% of helium (due to He glow discharges used for wall conditioning) and 3% of carbon (which comes from erosion from the plasma facing components). The electron temperature profile is such that these impurities are completely stripped in the confined plasma. The injected impurity ionization stage-resolved distribution used in NCLASS is that resulting from ITC. The results of the NCLASS calculations are shown in figure 8.

The uncertainties on the transport coefficients have been evaluated in the Al case. We have varied the temperature and density gradient profiles using the experimental T_i and n_i error bars (for the sake of simplicity, we have applied here the analytical formulae given in [18] which have been checked to match the NCLASS predictions in the present case). The relative error bar on the neoclassical diffusion coefficient thus obtained is about 2.5% over the whole profile, consistent with the absence of gradient dependence of neoclassical diffusion in the analytical predictions (see for example [18]). The error bar on the convection velocity, as indicated in figure 8, is about $0.1\,\mathrm{m\,s^{-1}}$ in the central part of the plasma and increases to $2\,\mathrm{m\,s^{-1}}$ in the outer part, due to the strong dependence of the Pfirsch–Schülter term on the normalized ion temperature and density gradients.

The neoclassical diffusion coefficient increases with the impurity charge up to Cr ($Z = 24$) and decreases when the impurity charge is increased further up to Ge ($Z = 32$). Nevertheless it is about one order of magnitude below the observed one everywhere in the plasma for all species (except possibly for Ge at $r/a < 0.1$). We thus conclude that impurity transport is anomalous in these experimental conditions. This result is in agreement with previous measurements of density fluctuations and particle transport studies in sawtoothing and sawtooth-free plasmas in Tore Supra [16].

The neoclassical convection velocity is close to 0 (or very slightly inward) for $r/a < 0.35$. Beyond this radius it tends to be outward over a narrow radius interval ($0.4 \lesssim r/a \lesssim 0.6$), then it is more and more unambiguously inward toward the plasma periphery (about $-3\,\mathrm{m\,s^{-1}}$ at $r/a \simeq 0.8$). Inside $r/a = 0.42$ the calculated values are too low to reveal a Z dependence, while beyond this radius the inward convection seems to weaken as Z is increased. The experimental values are also weak in the central plasma but the comparison with theoretical predictions is disputable because of the large uncertainties of both the experimental (except for N) and the theoretical values. We thus lack a better experimental determination of the heavier species convection velocity.

4.2. *Quasilinear gyrokinetic simulations*

For theoretical predictions of turbulent transport we have used the quasilinear, gyrokinetic, fixed-gradient code QuaLiKiz [7] in the region where the density and temperature gradients are determined with a sufficient accuracy. These gyrokinetic simulations use the same input profiles as the NCLASS runs (see section 4.1). The CRONOS simulations (figures 9(*a*) and (*b*)) have then been taken as an input to the Kinezero code [19] to study the nature of turbulence in our plasmas. The uncertainty on the ion temperature gradient has been studied in a previous publication [12], where it is shown that within a 30% $\nabla T_i/T_i$ variation the results remain qualitatively the same. As can be seen in figure 9 turbulence is dominated by the ion temperature gradient (ITG) modes.

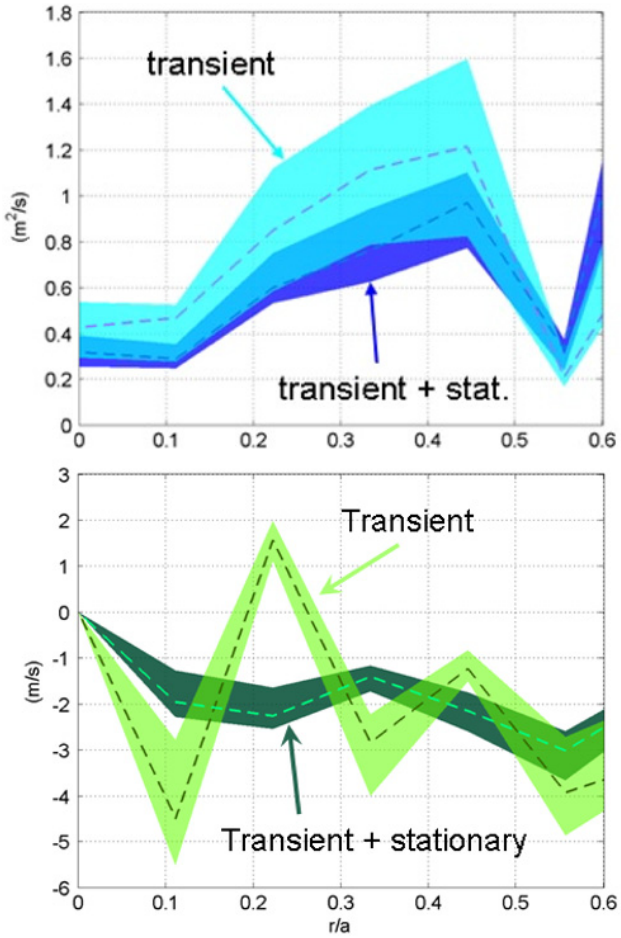

Figure 7. Radial profiles of (top) diffusion coefficient and (bottom) convection velocity determined from (light shade) a transient alone and (dark shade) combined analysis of a transient and a stationary case.

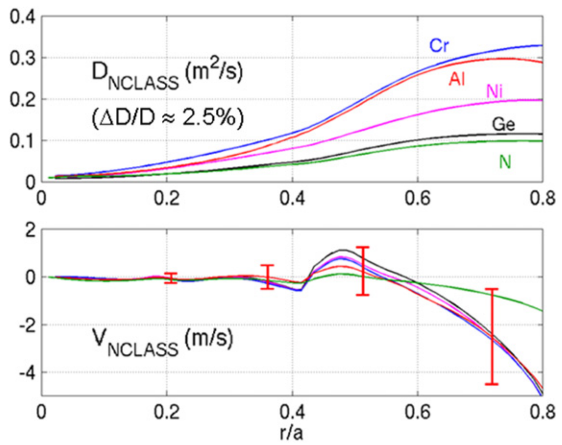

Figure 8. Neoclassical diffusion coefficient (top) and convection velocity (bottom) calculated with NCLASS for all injected impurities. See text for the error bar evaluation.

The turbulent fluxes of the injected impurities are calculated with QuaLiKiz, which is able to handle three species at the same time: electrons, main ions and a single impurity species. The impurity charge is assumed not to vary along the plasma minor radius, which is strictly verified for the lighter species and in reasonable agreement with the weak charge variation of the heavier species in the core plasma ($r/a \leqslant 0.8$), as deduced from the experimental impurity density profiles determined by the ITC code. The saturation level is arbitrary. The values of the transport coefficients are thus obtained in relative units. The values in absolute units can be obtained by multiplying the code results by a single factor. In order to make the comparison easier in this study, this factor has been chosen such that the modelled diffusion coefficient matches approximately the observed one in the range $0.25 \leqslant r/a \leqslant 0.5$ (note that this is not very different from using the V/D ratio, but in addition it allows us to compare the experimental and modelled profile shapes of D and V individually).

The predicted turbulent diffusion (figure 10, top right) does not exhibit any clear Z dependence, due to the fact that both the trapped and the passing impurity contributions are independent of Z. The diffusion coefficient increases from the plasma centre to the periphery, as expected from the gradients and in agreement with the experimental results. There is no turbulent diffusion at the very centre due to the fact that the n_e and T_e gradients are constrained to 0 at $r/a = 0$. The sharp transition at $r/a \simeq 0.6$ and the very high diffusion values at $r/a \geqslant 0.6$ are probably due to an overestimate of the input gradients and to the stiff response of the flux to the gradient above the turbulence threshold. It could also explain the somewhat high diffusion values in the range $0.1 \leqslant r/a \leqslant 0.25$ compared with the neighbouring range $0.25 \leqslant r/a \leqslant 0.55$. This demonstrates the crucial role of accurate gradient measurements along with reliable turbulence threshold modelling.

The comparison of the sign and profile shape of the predicted neoclassical (figure 8, bottom) and turbulent (figure 10, bottom right) convection velocities with the most accurately determined experimental convection velocity (nitrogen) indicates that the latter is more consistent with the turbulent convection modelled by the quasilinear gyrokinetic calculations. As in the sawtooth-free, LH heated case [12], it is inward in the whole plasma, and increases in absolute value toward the plasma periphery. In agreement with more general results obtained with the nonlinear gyrofluid model TRB [20], the curvature-compressibility flux is inward and dominates over the thermodiffusion flux in the whole plasma. As only the latter flux is predicted to depend on the impurity charge (see also [21]), no charge dependence is expected in the present experimental situation. Despite the fact that the convection velocity is inward, the stationary impurity density gradient length ($(\nabla n_Z/n_Z)^{-1} = D/V$, of the order of 1 m in the radial range $0.1 \leqslant r/a \leqslant 0.6$) deduced from the experimental transport coefficient ratio is longer than the electron density gradient length (of the order of 0.33 m in the same radial range) due to the large turbulent diffusion coefficient. The impurity density profiles are thus less peaked than the electron density profile, which is favourable to minimization of radiation loss and fuel dilution.

5. Conclusion

The impurity transport analysis has been optimized in the case of ohmic, weakly sawtoothing plasmas over an extended

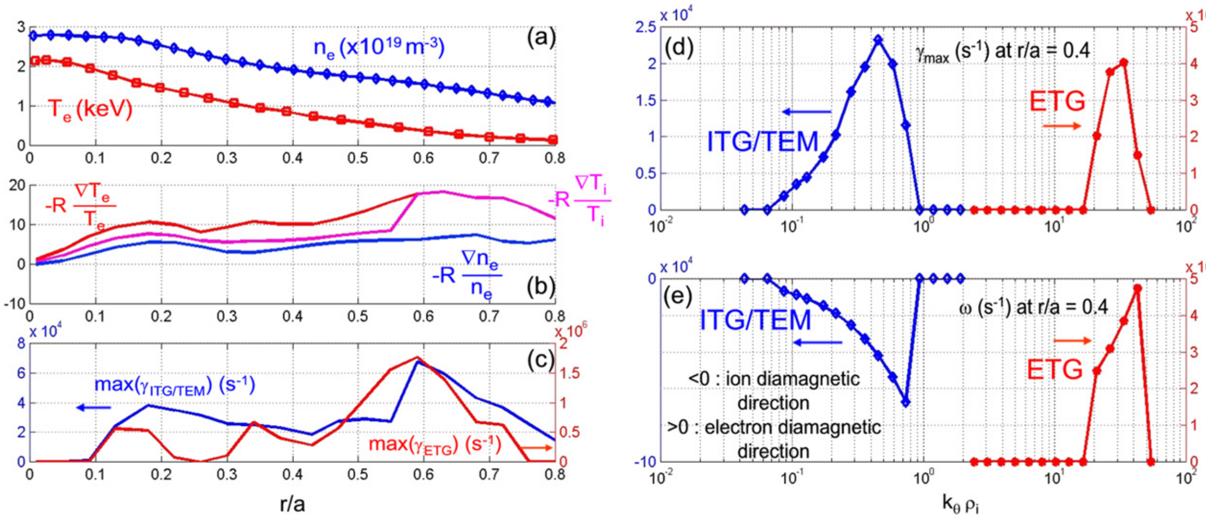

Figure 9. (*a*) Experimental n_e and T_e radial profiles. (*b*) Normalized gradients used for QuaLiKiz simulations (from CRONOS code). Kinezero calculation of (*c*), (*d*) maximal growth rate γ for ITG/TEM and ETG turbulence modes, (*e*) mode frequency.

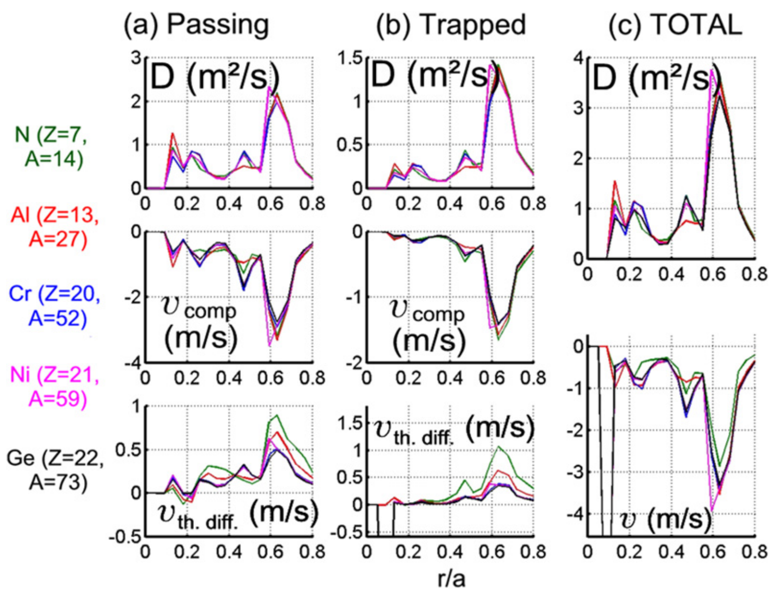

Figure 10. Quasilinear gyrokinetic simulations of transport coefficients by QuaLiKiz. (*a*) Passing impurities, (*b*) trapped impurities and (*c*) total.

impurity charge range (7–30). For the lightest species, nitrogen, a new technique has been developed: the supersonic pulsed injection of trace impurities. This technique provides a source term much shorter than the impurity transport characteristic time, which is shown to improve dramatically the diffusion coefficient determination compared with a slower technique. We have also shown that the convection velocity determination from this technique or from laser blow-off injections can be improved by combining the analysis of a transient with that of a stationary injection of the same species. The resulting uncertainty on the convection determination drops to about 0.5 m s^{-1}.

The best method (combined analysis of supersonic injections and stationary injections) provides a diffusion coefficient much higher than the neoclassical prediction. It increases smoothly from a few tenths of m^2 s^{-1} in the plasma centre up to around 4 m^2 s^{-1} in the outer half of the plasma. As predicted by the gyrokinetic quasilinear simulations of turbulent impurity transport, no Z dependence is observed. It has to be noticed, however, that the experimental nitrogen diffusion coefficient lies below those of the heavier species.

The agreement between the experimental and the modelled profile shapes of V is satisfactory. The convection velocity is inward in agreement with the weak neoclassical velocity predicted by NCLASS and the inward turbulent velocity predicted by gyrokinetic quasilinear simulations. This is attributed to the curvature flux term, which is much stronger than thermodiffusion in the investigated situation. Despite this inward convection, transport is such that the impurity density profiles are less peaked than the electron density profile, a consequence of the large turbulent diffusion coefficient. This stresses that turbulence may be a useful tool in the future in order to minimise the plasma core contamination in a fusion reactor.

Acknowledgments

This work, supported by the European Communities under the contract of Association between EURATOM and CEA, was carried out within the framework of the European Fusion Development Agreement. The views and opinions expressed herein do not necessarily reflect those of the European Commission.

References

[1] Guirlet R. *et al* 2006 *Plasma Phys. Control. Fusion* **48** B63
[2] Scavino E. *et al* 2003 *Plasma Phys. Control. Fusion* **45** 1961
[3] Giannella R. *et al* 1994 *Nucl. Fusion* **34** 1185
[4] Weiland J. *et al* 1992 *Nucl. Fusion* **32** 151
[5] Kinsey J. *et al* 2005 *Phys. Plasmas* **12** 052503
[6] Candy J. *et al* 2003 *J. Comput. Phys.* **186** 545
[7] Bourdelle C. *et al* 2007 *Phys. Plasmas* **14** 112501
[8] Puiatti M.E. *et al* 2006 *Phys. Plasmas* **13** 042501
[9] Angioni C. *et al* 2007 *Plasma Phys. Control. Fusion* **49** 2027
[10] Giroud C. *et al* 2007 *Nucl. Fusion* **47** 313
[11] Bucalossi J. *et al* 2002 *29th EPS Conf. on Plasma Physics Controlled Fusion (Montreux, Switzerland, 2002)* http://epsppd.epfl.ch/Montreux/pdf/O2_07.pdf
[12] Parisot Th. *et al* 2008 *Plasma Phys. Control. Fusion* **50** 055010
[13] Lopes-Cardozo N.J. *et al* 1995 *Plasma Phys. Control. Fusion* **37** 799
[14] Mattioli M. *et al* 1998 *Nucl. Fusion* **38** 1629
[15] Houlberg W.A. *et al* 1997 *Phys. Plasmas* **4** 3230
[16] Sabot R. *et al* 2006 *Plasma Phys. Control. Fusion* **48** 421
[17] Basiuk V. *et al* 2003 *Nucl. Fusion* **43** 822
[18] Wenzel K.W. and Sigmar D.J. 1990 *Nucl. Fusion* **30** 1117
[19] Bourdelle C. *et al* 2002 *Nucl. Fusion* **42** 892
[20] Dubuit N. *et al* 2007 *Phys. Plasmas* **14** 042301
[21] Angioni C. *et al* 2006 *Phys. Rev. Lett.* **96** 095003